

See discussions, stats, and author profiles for this publication at: <https://www.researchgate.net/publication/231633704>

Monte Carlo Simulation of Defect-Free Cross-Linked Polyelectrolyte Gels†

ARTICLE *in* THE JOURNAL OF PHYSICAL CHEMISTRY B · JULY 2003

Impact Factor: 3.3 · DOI: 10.1021/jp022336w

CITATIONS

51

READS

26

2 AUTHORS, INCLUDING:



Stefanie Schneider

RWTH Aachen University

13 PUBLICATIONS 354 CITATIONS

SEE PROFILE

Monte Carlo Simulation of Defect-Free Cross-Linked Polyelectrolyte Gels[†]

Stefanie Schneider* and Per Linse

Physical Chemistry 1, Center for Chemistry and Chemical Engineering, Lund University,
P.O. Box 124, S-221 00 Lund, Sweden

Received: October 30, 2002; In Final Form: March 3, 2003

Model systems of cross-linked polyelectrolyte gels were investigated by means of Monte Carlo simulations. The model contained a charged defect-free three-dimensional network of a diamond-like topology and explicit counterions. Pressure vs volume relations and chain extensions were determined and compared to those of the corresponding polyelectrolyte solution. The structure of the gel was characterized by radial distribution functions. In the swollen state, the network particles and the counterions are inhomogeneously distributed in space. Also, the properties of the polyelectrolyte gels were investigated at different charge density, cross-linking density, chain flexibility, and counterion valence. An increase in the gel volume was observed for increasing charge density, decreasing cross-linking density, and increasing chain stiffness. The exchange of the monovalent counterions for divalent counterions reduced the equilibrium volume of the gel substantially. The affine assumption, which states that a linear relation exists between chain end-to-end separation and macroscopic gel size, was found to be only of limited validity, whereas the Gaussian chain approximation was never fulfilled for polyelectrolyte gels.

Introduction

Polyelectrolyte gels consist of charged polymer networks, counterions, and solvent, and they are usually synthesized by chemically cross-linking charged or titrating polymers. They have been extensively studied experimentally during the past decades.¹ Initial work mainly focused on the swelling behavior in solutions of simple salt.^{2,3} More recent investigations also address many other issues, e.g., the influence of oppositely charged surfactants^{4–8} and microgel particles.^{9,10} Polyelectrolyte gels can take up large amounts of water (up to several hundred times their dry mass) and are therefore used as superabsorbents in hygiene products and for drug delivery.¹

Due to the condition of macroscopic electroneutrality, the counterions of the charged network have to be confined inside the gel volume. The large swelling capacity of polyelectrolyte gels is attributed to the increase of the counterion entropy as the volume available to the ions is increased.^{11,12} The degree of swelling is determined by the composition of the network and the surrounding solution. Whereas the relative amount of cross-linkers can be well-controlled experimentally, the topology of the network (as characterized by the chain length distribution, the frequency and length distribution of free ends, and the frequency and type of entanglements) is far more difficult to control or even to determine. Furthermore, it is strongly dependent on the conditions at preparation time. Solution properties are easy to control, and typically addition of salt,¹³ multivalent ions, and oppositely charged surfactants^{14,15} lead to a reduction of the gel volume.

The earliest molecularly based theories of polymer networks originate from Flory and Rehner^{16,17} and Wall¹⁸ (affine model) and from James and Guth^{19,20} (phantom model) and treat uncharged networks using mean-field approaches. The base for the calculation of the network free energies in these models

was the analogy between the network chains and elastic springs. Excluded volume was not taken into account in these models. The free energy was calculated as the sum of a liquidlike contribution (interaction between the network segments) and an elastic contribution related to the configurational entropy of the chains. Later, tube models^{21,22} and the constrained junction model by Flory and Erman^{23,24} tried to account for excluded volume interactions between network chains. This work was nicely summarized by Kenkare et al.²⁵ Rubinstein and Panyukov extended the tube model by allowing for a non-affine change of the tube diameters on network deformation.²⁶

Khokhlov and co-workers were studying the swelling of polyelectrolyte and polyampholyte gels in pure solvent, in the presence of salt, in mixed solvents, and in the presence of other macroions, e.g., surfactant micelles. A large part of the research of his group was collected in a review article.²⁷ In addition to the interaction of the network with the solvent and the elastic contribution from the network elasticity, an entropy term from the free motion of the counterions and an electrostatic term using the Debye–Hückel approximation were used to calculate the free energy of the network. The equilibrium swelling was found from the condition of equal osmotic pressures and equal chemical potentials inside and outside the gel. Most theories are based on ideal networks, which are, as mentioned above, hard to reproduce experimentally. Therefore, computer modeling of these kinds of systems will be very useful for the evaluation of theoretical work.

The literature on the simulation of uncharged networks is extensive and was recently reviewed by Escobedo and de Pablo.²⁸ In addition to the work reviewed there, Kenkare et al.²⁵ investigated the pressure vs volume relation of polymer networks composed of hard spheres. Escobedo and de Pablo²⁹ as well as Ayt and Hentschke³⁰ studied the swelling of a similar model network with explicit solvent molecules, and Gilra et al.³¹ investigated the properties of a network using the bond fluctuation model on a simple cubic lattice.

[†] Part of the special issue "International Symposium on Polyelectrolytes".

* To whom correspondence should be addressed. E-mail: Stefanie.Schneider@fkem1.lu.se.

Simulations of charged cross-linked gels are however rare. The long-range nature of the electrostatic interactions creates additional difficulties in the simulation of charged gels. In 1996, Aalberts³² performed the first simulation of a polyelectrolyte gel by using a two-dimensional finite lattice model. The effect of the counterions was included by introducing a counterion or hydrogen ion pressure term in the model. Subsequently, Barenbrug et al. determined the free energy of a single polyelectrolyte chain on a lattice using a screened Coulomb potential³³ and used the result to calculate the equilibrium swelling of a gel composed of several chains connected by tetrafunctional nodes.³⁴ Both papers do not describe the charged gel and its counterions on an equal level of complexity.

In this contribution, we present properties of polyelectrolyte gels obtained by Monte Carlo (MC) simulations using a model that describes the network charges and the counterions on an equal level of simplification. Similar to Escobedo and de Pablo,³⁵ we chose a network with a diamond-like topology. All chains are of equal length, and no loose ends or entanglements occur. The counterions as well as the network charges are described by charged hard spheres. The long-ranged electrostatic interactions were included by using the Ewald summation technique,^{36,37} which is used frequently in the simulation of charged systems, e.g., linear polyelectrolyte chains³⁸ and charged colloids.³⁹ In a previous communication,¹² we used this approach to examine a polyelectrolyte gel and compared its swelling ability with that of a corresponding uncharged network. In particular, the presence of the counterions and the role of the electrostatic interactions were discussed. In the present contribution, we focus on a comparison between the properties of a polyelectrolyte gel and the corresponding polyelectrolyte solution, the structure of a polyelectrolyte gel, and the swelling behavior of a polyelectrolyte gel at different conditions.

Our results include the pressure vs volume relation and chain stretching for a polyelectrolyte gel and the corresponding polyelectrolyte solution as well as the structure of a polyelectrolyte gel, which is investigated in detail using radial distribution functions. It will be shown that the counterions are not homogeneously distributed in the gel as commonly assumed even in recent theories.⁴⁰ We also examine how properties of a polyelectrolyte gel depend on the chain linear charge density, the cross-linking density, the chain flexibility, and the counterion valence. Finally, we compare the results with experimental observations.

Method

Model. The polyelectrolyte gel is described within the primitive model. All charged species are treated explicitly as charged hard spheres, and the solvent enters the model only through its permittivity. The polymer chains are modeled as a sequence of charged hard spheres (beads) connected by harmonic bonds. The interconnectivity of the network is realized by connecting the ends of the chains with harmonic bonds to tetrafunctional charged cross-linkers (nodes). For simplicity, we employ a defect-free network with a diamond-like topology in which all the chains are of equal length (see Figure 1). The topology of the network is unchanged throughout the simulation, thus representing a covalently cross-linked network. A harmonic angular potential regulates the flexibility of the charged chains. The angle formed by connected bead–node–bead particles is, however, kept fully flexible.

The network contains N_{node} nodes and N_{chain} chains, the latter composed of n_{bead} beads each. Thus, the total number of beads, N_{bead} , is given by $N_{\text{bead}} = N_{\text{chain}} n_{\text{bead}}$ and the total number of

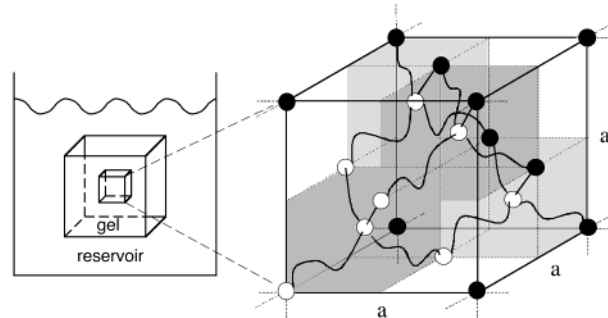


Figure 1. (left) Schematic illustration of a macroscopic gel in a reservoir of solvent. (right) Schematic illustration of one unit cell of a defect-free network of diamond-like topology containing eight tetrafunctional nodes (open spheres) linked by noncrossing chains (wavy lines). Note that four of the eight subcubes contain chains (shaded) whereas the other four are empty.

network particles, N_{network} , is given by $N_{\text{network}} = N_{\text{node}} + N_{\text{bead}}$. The fraction of nodes in the network is defined as $x_{\text{node}} = N_{\text{node}}/N_{\text{network}}$. In addition to the network, the gel also contains N_{ion} unconnected charged counterions making the gel electroneutral, and thus, the gel is described by $N = N_{\text{network}} + N_{\text{ion}}$ particles.

The total potential energy of the system, U , is the sum of a nonbonded potential energy (Coulomb interaction and hard-core repulsion), U_{nonbond} , a bond potential energy, U_{bond} , and an angular potential energy, U_{angle} , according to

$$U = U_{\text{nonbond}} + U_{\text{bond}} + U_{\text{angle}} \quad (1)$$

The nonbonded potential energy is assumed to be pairwise additive, according to $U_{\text{nonbond}} = \sum_{i < j} u_{ij}(r_{ij})$, with the interaction potential, u_{ij} , for pair ij , where i and j denote either a bead, a node, or a counterion, given by

$$u_{ij}(r_{ij}) = \begin{cases} \infty, & r_{ij} < R_i + R_j \\ \frac{z_i z_j e^2}{4\pi\epsilon_0\epsilon_r r_{ij}}, & r_{ij} \geq R_i + R_j \end{cases} \quad (2)$$

where z_i is the charge of particle i , R_i is the radius of particle i , e is the elementary charge, ϵ_0 is the permittivity of vacuum, ϵ_r is the relative permittivity of the solvent, and $r_{ij} = |\mathbf{r}_{ij}| = |\mathbf{r}_i - \mathbf{r}_j|$ is the distance between particle i and j with \mathbf{r}_i denoting the position of particle i . The bond potential energy is given by

$$U_{\text{bond}} = \sum_{m=1}^{N_{\text{bond}}} \frac{k_{\text{bond}}}{2} (r_{m,\text{bond}} - r_0)^2 \quad (3)$$

where N_{bond} is the number of bonds in the network and $r_{m,\text{bond}}$ is the bond length of bond m with $r_0 = 0.5$ nm being the equilibrium bond length and $k_{\text{bond}} = 0.4$ N/m the force constant. With the other interactions included, the root-mean-square (rms) bead–bead separation, $\langle R_{\text{bb}}^2 \rangle^{1/2}$, was typically 0.6 nm. Here, and below, $\langle \dots \rangle$ denotes an ensemble average. The angular potential energy is given by

$$U_{\text{angle}} = \sum_{m=1}^{N_{\text{chain}}} \sum_{i=2}^{n_{\text{bead}}-1} \frac{k_{\text{angle}}}{2} (\alpha_{i \in m} - \alpha_0)^2 \quad (4)$$

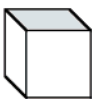
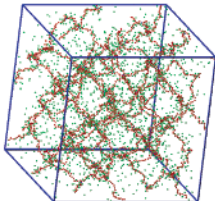
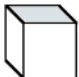
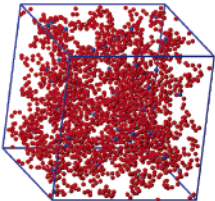


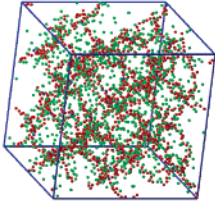
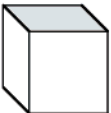
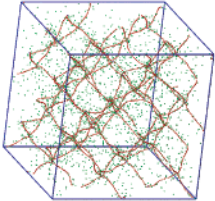
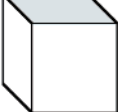

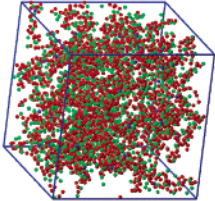
where N_{chain} is the number of polymer chains, n_{bead} is the number of beads per chain, k_{angle} is the force constant, and $\alpha_{i \in m}$ is the bond angle formed by three consecutive beads in chain m with bead i as the central one and $\alpha_0 = 180^\circ$ being the equilibrium angle. The angular force constant was selected between 0 and

TABLE 1: General Data of the Model

box length	$L = 5.0 - 35$ nm
bead radius	$R_{\text{bead}} = 0.2$ nm
node radius	$R_{\text{node}} = 0.2$ nm
counterion radius	$R_{\text{ion}} = 0.2$ nm
bead charge	$z_{\text{bead}} = 0, 0.5, \text{ and } 1.0$
node charge	$z_{\text{node}} = 0, 0.5, \text{ and } 1.0$
counterion charge	$z_{\text{ion}} = -1.0 \text{ and } -2.0$
chain persistence length	$l_p = 0.70 - 37$ nm
fraction of nodes	$x_{\text{node}} = 0.025 \text{ and } 0.050$
number of beads per chain	$n_{\text{bead}} = 10 \text{ and } 20$
temperature	$T = 298$ K
relative permittivity	$\epsilon_r = 80$

8.3×10^{-23} J/(deg)² to vary the intrinsic stiffness of the chains. In addition to the angular potential, the electrostatic interaction among the charged polymer beads and counterions contributes to the stiffness of the polymer chain. The intrinsic chain stiffness is characterized by the bare persistence length, l_p , of the chain, which was determined in separate simulations of the corresponding linear and uncharged chains. The persistence lengths were evaluated by using the projection length, $l_p = \langle R_{bb}^2 \rangle^{1/2} / (1 - \langle \cos \theta \rangle)$, which is the projection of the end-to-end vector on the direction of the first bond, and where $\theta = \pi - \alpha$ is the angle between the bond vectors of two consecutive bonds.^{41,42}

TABLE 2: Simulated Systems and Their Properties

specifications	relative size at $P = 0$	snapshots ^{a)}
Reference gel $z_{\text{bead}} = 1$ $x_{\text{node}} = 0.025$ $n_{\text{bead}} = 20$ $N_{\text{bead}} = 320$ $k_{\text{angle}} = 0.00 \cdot 10^{-24}$ J/(deg) ² $l_p = 0.70$ nm $z_{\text{ion}} = -1$ $N_{\text{ion}} = 328$	ref 	ref 
Gel I (decreased linear charge density) as reference gel but $z_{\text{bead}} = 0.5$ $N_{\text{ion}} = 164$	Ia 	Ib 
Gel Ib (uncharged gel) as reference gel but $z_{\text{bead}} = 0$ $N_{\text{ion}} = 0$	Ib 	
Gel II (increased crosslinking density) as reference gel but $x_{\text{node}} = 0.05$ $n_{\text{bead}} = 10$ $N_{\text{bead}} = 160$ $N_{\text{ion}} = 168$	II 	II 
Gel IIIa (increased chain stiffness) as reference gel but $k_{\text{angle}} = 8.30 \cdot 10^{-24}$ J/(deg) ² $l_p = 4.0$ nm	IIIa 	IIIb 
Gel IIIb (increased chain stiffness) as reference gel but $k_{\text{angle}} = 83.0 \cdot 10^{-24}$ J/(deg) ² $l_p = 37$ nm	IIIb 	
Gel IV (divalent counterions) as reference gel but $z_{\text{ion}} = -2$ $N_{\text{ion}} = 164$	IV 	IV 
The polyelectrolyte solution contains 16 flexible charged polymer chains, with 20 beads each ($n_{\text{bead}} = 20$, $N_{\text{bead}} = 320$, $z_{\text{bead}} = 1$) and 320 counterions ($N_{\text{ion}} = 320$, $z_{\text{ion}} = -1$). In addition to that, it contains also eight positive and eight negative small ions corresponding to the nodes and their counterions in the gel.		

^{a)} The snapshots display nodes (blue dots), beads (red dots), and counterions (green dots). They are obtained for equilibrium with pure solvent and 8-fold larger systems than those described in the specifications.

Seven different gels have been considered. One of them will be referred to as the *reference system*, in which the network carries $z_{\text{bead}} = 1$ charge per bead, the node fraction is $x_{\text{node}} = 0.025$ giving $n_{\text{bead}} = 20$ beads per chain, the chains are fully flexible, $k_{\text{angle}} = 0 \text{ J/deg}^2$, and in which the gel contains monovalent counterions, $z_{\text{ion}} = -1$. As compared to the reference system, (i) systems Ia and b have reduced or zero network charge, $z_{\text{bead}} = z_{\text{node}} = 1/2$ and 0, respectively, (ii) system II contains a higher fraction of nodes, $x_{\text{node}} = 0.050$ corresponding to $n_{\text{bead}} = 10$, (iii) systems IIIa and b possess chains with increased bare stiffness, $k_{\text{angle}} > 0 \text{ J/deg}^2$, and (iv) system IV contains divalent counterions, $z_{\text{ion}} = -2$. Moreover, a polyelectrolyte solution related to the reference gel system has been examined. Throughout, $R_{\text{bead}} = R_{\text{node}} = R_{\text{ion}} = 0.2 \text{ nm}$, $T = 298 \text{ K}$, and $\epsilon_r = 80$ have been used. Table 1 provides general data of the simulations, whereas specific data, bare persistence lengths, and some snapshots of the systems are provided in Table 2.

Pressure and Equilibrium Volume. For a system with central and pairwise additive potentials, the osmotic pressure can be expressed as the sum of the ideal pressure, a virial term, and a contact term,³⁷ according to

$$P = P_{\text{ideal}} + P_{\text{virial}} + P_{\text{contact}} \quad (5)$$

The ideal contribution is given by the ideal gas law $P_{\text{ideal}} = \rho k_B T$, with $\rho = N/V$, where V is the volume of the system, N the total number of particles in the system, k_B the Boltzmann constant, and T the temperature. The virial contribution becomes

$$P_{\text{virial}} = \frac{1}{3V} \left\langle \sum_i \sum_{j>i} \mathbf{r}_{ij} \cdot \mathbf{f}_{ij} \right\rangle \quad (6)$$

where \mathbf{f}_{ij} is the force acting between particles i and j .³⁷ The contact term arises from the infinite potential appearing at hard-sphere contacts and is given by

$$P_{\text{contact}} = \frac{2\pi}{3} k_B T \sum_i \sum_j (R_i + R_j)^3 \rho_i \rho_j g_{ij}(R_i + R_j) \quad (7)$$

where $\rho_i = N_i/V$ is the number density of particle i and $g_{ij}(R_i + R_j)$ is the radial distribution function (rdf) between pair ij at contact separation, $R_i + R_j$. In practice, the contact term is obtained by extrapolating $g_{ij}(r)$ to the contact distance $r = R_i + R_j$. The contribution from the angular potential to the pressure is identical, zero, and therefore, eqs 5–7 are applicable for the pressure evaluation of the present model system. The network packing fraction, η_{network} , used below, is conventionally defined as $\eta_{\text{network}} \equiv (4\pi/3)R^3 \rho_{\text{network}}$, with $\rho_{\text{network}} = N_{\text{network}}/V$ and $R = R_{\text{bead}} = R_{\text{node}}$.

A solvent-swollen gel, containing a charged network, counterions, and solvent only, is in equilibrium with the surrounding solution (reservoir) when the osmotic pressure in the gel is equal to that in the reservoir. If the reservoir contains pure solvent only, its osmotic pressure is zero by definition and the equilibrium volume of the gel, V_{eq} , is the volume at which the osmotic pressure inside the gel is zero. However, if the reservoir comprises a solute that cannot penetrate the gel, e.g., a high molecular weight polymer, higher equilibrium pressures are attainable. Finally, if simple salt is present, not only the osmotic pressure but also the chemical potential of the salt has to be equal in the gel and reservoir phases.

Simulation Details. The properties of the gels were obtained by performing MC simulations in the canonical ensemble

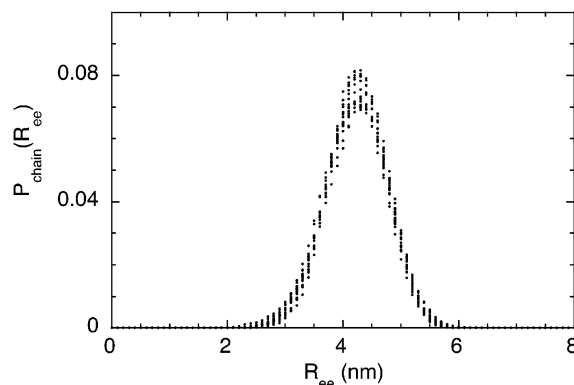


Figure 2. Chain end-to-end distance distribution functions, $P_{\text{chain}}(R_{\text{ee}})$, of the 16 individual chains for system II at $\eta_{\text{network}} = 0.068$ corresponding to $P/\rho k_B T \approx 0.1$.

applying the Metropolis algorithm.^{37,43} The particles were enclosed in a cubic box and in order to account for the macroscopic nature of a gel, periodic boundary conditions were applied. Initially, the nodes were positioned on a diamond lattice and connected by nonentangled chains. The counterions were placed randomly. During the simulations all particles were moved in the configurational space. Each system comprised typically one unit cell containing $N_{\text{node}} = 8$ nodes and $N_{\text{chain}} = 16$ chains. Some simulations with an 8-fold larger number of unit cells were performed to examine system size effects and to obtain structural information.

The long-ranged electrostatic interactions were handled by using the Ewald summation technique with conducting boundary conditions.^{36,37,44,45} The cutoff parameters were selected such that the truncation error of the Ewald summation was smaller than $1 \times 10^{-6} \text{ kJ/mol}$. This error was several orders of magnitude smaller than the statistical uncertainty of the total potential energy of the system ($\approx 1 \times 10^{-3} \text{ kJ/mol}$).

Each production run of 10^5 – 10^6 MC passes (attempted moves per particle) was preceded by an equilibration run of 2.5×10^5 passes. Among nodes, beads, and counterions, the tetrafunctional nodes are expected to display the slowest mobility in the configurational space. The ergodicity of the simulations was assessed by examining the distribution functions of individual chain end-to-end distances, $P_{\text{chain}}(R_{\text{ee}})$. Figure 2 shows that all distribution functions for the 16 chains in system II at a packing fraction $\eta_{\text{network}} = 0.0068$, corresponding to $P/\rho k_B T \approx 0.1$, collapse nearly onto a single curve. Thus, the mobility of the nodes is sufficient to make all chains equivalent, and the sampling of the configurational space is therefore most likely ergodic. The relatively low packing fraction of network particles and the use of flexible bonds make the mobility in the configurational space considerably larger than in many previous simulations of uncharged gels. Thus, the use of more advanced methods for obtaining trial configurations involving chain deletion and regrowth⁴⁶ is not necessary.

The statistical uncertainty is given as one standard deviation of the mean and was estimated by dividing the simulations into 15 subbatches. The estimated precision of the reduced pressure lies between 4×10^{-4} and 5×10^{-3} . Error bars are omitted in the figures because the errors are always much smaller than the symbols. The simulations were performed by using the integrated Monte Carlo/molecular dynamics/Brownian dynamics simulation package MOLSIM,⁴⁷ after extending it to cross-linked systems.

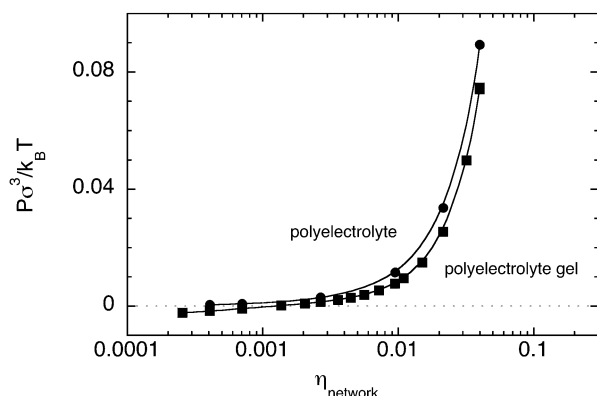


Figure 3. Pressure, $P\sigma^3/k_B T$, as a function of the network packing fraction, η_{network} , for the reference system (labeled “polyelectrolyte gel”) and the corresponding polyelectrolyte solution (labeled “polyelectrolyte”). For the polyelectrolyte gel, the abscissa denotes the polyion packing fraction. The pressure of a pure reservoir is also given (dotted line).

Results and Discussion

Pressure vs packing fraction relations and chain stretching of the reference system and the corresponding polyelectrolyte solution will first be examined. Thereafter, we will discuss the structure of the reference system using radial distribution functions. In addition, the effect of systematic variations of the chain linear charge density, the cross-linking density, the chain bare stiffness, and the valence of the counterions on pressure-packing fraction relations and chain extension will be considered. Snapshots of the systems in equilibrium with pure solvent as well as the relative gel sizes are depicted in Table 2.

Reference Gel and Corresponding Polyelectrolyte Solution. A typical configuration of the reference gel in equilibrium with pure solvent is shown in Table 2. The beads (red dots) form fairly stretched chains, which are connected by the nodes (blue dots) forming a regular and open network. The counterions seem to be accumulated near the oppositely charged beads and nodes.

Figure 3 displays the pressure of the reference system and the corresponding polyelectrolyte solution expressed in units of $k_B T/\sigma^3$ as a function of the network packing fraction η_{network} . In the dilute regime, the osmotic pressure is close to zero, whereas it increases rapidly with increasing packing fraction in the more concentrated regime. Moreover, in the polyelectrolyte gel, the pressure (i) is lower than in the corresponding polyelectrolyte solution at all packing fractions and (ii) becomes negative at sufficient dilution. Due to the extended packing fraction range considered and the concomitant large variation in the pressure, the pressure will in the following be given in units of the ideal pressure of the corresponding system with all particles disconnected, $\rho k_B T$. Such a representation leads to an expansion of the curves at low packing fractions and a compression at high packing fractions.

The reduced pressure, $P/\rho k_B T$, of the reference system is displayed in Figure 4a as a function of the network packing fraction, η_{network} . This plot displays three different regimes that are typical for polymer networks.²⁸ At low packing fractions (regime I), the pressure is negative and increases as η_{network} is increased. In this regime, the dominating contribution to the pressure comes from the stretching of the network chains appearing in the virial term. Hence, the connectivity of the network limits the expansion of the gel. A gel expanded to a volume corresponding to a negative pressure, e.g., by a mechanical force, would spontaneously contract when the force

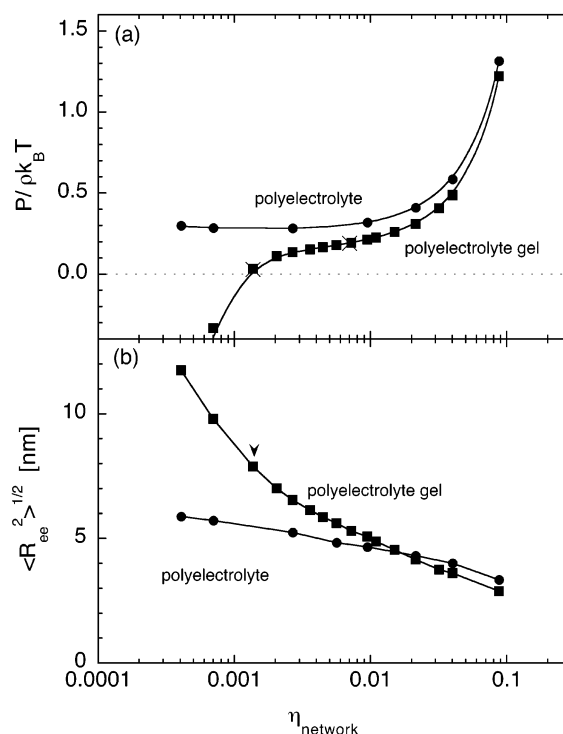


Figure 4. (a) Reduced pressure, $P/\rho k_B T$, and (b) rms end-to-end chain distance, $\langle R_e^2 \rangle^{1/2}$, as a function of the network packing fraction, η_{network} , for the reference system (labeled “polyelectrolyte gel”) and the corresponding polyelectrolyte solution (labeled “polyelectrolyte”). For the polyelectrolyte gel, the abscissa denotes the polyion packing fraction. In part a, pressures from an 8-fold larger gel system are also given (two crosses) but barely visible. In part b, the packing fractions at which $P = 0$ is indicated by an arrow.

TABLE 3: Equilibrium Network Packing Fractions $\eta_{\text{network,eq}}$ and Equilibrium Expansion Ratios Q_{eq}^a for the Reference System and Systems I–IV

system	ref	Ia	Ib	II	IIIa	IIIb	IV
$\eta_{\text{network,eq}}$	0.0013	0.0023	0.029	0.0044	0.00073	0.00049	0.010
Q_{eq}	290	220	25	84	510	760	47

^a $Q_{\text{eq}} = V_{\text{eq}}/V_{\text{dry}}$, where $V_{\text{dry}} = N(4\pi/3)R^3/0.7405$ denotes the volume occupied by the N particles in a close-packed structure. The bead size was selected to provide reasonable Coulomb interaction rather than reasonable excluded volume effects of the chain segments. Hence, in comparison with experiments the simulated Q_{eq} are exaggerated.

is released. In an intermediate regime (regime II), the reduced pressure is close to zero and stays nearly constant. In the reference system, $P/\rho k_B T$ is approximately 0.2 over a 10-fold variation of η_{network} . At high packing fractions (regime III), the pressure is positive and increases rapidly as η_{network} is increased. In this regime, the reduced pressure is dominated by excluded volume effects appearing in the contact term. The equilibrium packing fraction, $\eta_{\text{network,eq}}$, and the equilibrium expansion factor, Q_{eq} , the latter denoting the volume ratio of the swollen to the dry gel, are provided in Table 3. For the reference gel we obtained $Q_{\text{eq}} = 290$.

The pressure of the corresponding polyelectrolyte solution, obtained by disconnecting the chains from the nodes, is also included in Figure 4a (circles). At high packing fractions (regime III), there is only a small difference in the pressure between the polyelectrolyte solution and the polyelectrolyte gel, demonstrating that the 3D-connectivity is of minor importance in this regime. However, as the packing fraction is decreased, the reduced pressure of the polyelectrolyte solution decreases slower than that of the polyelectrolyte gel and the reduced pressure of

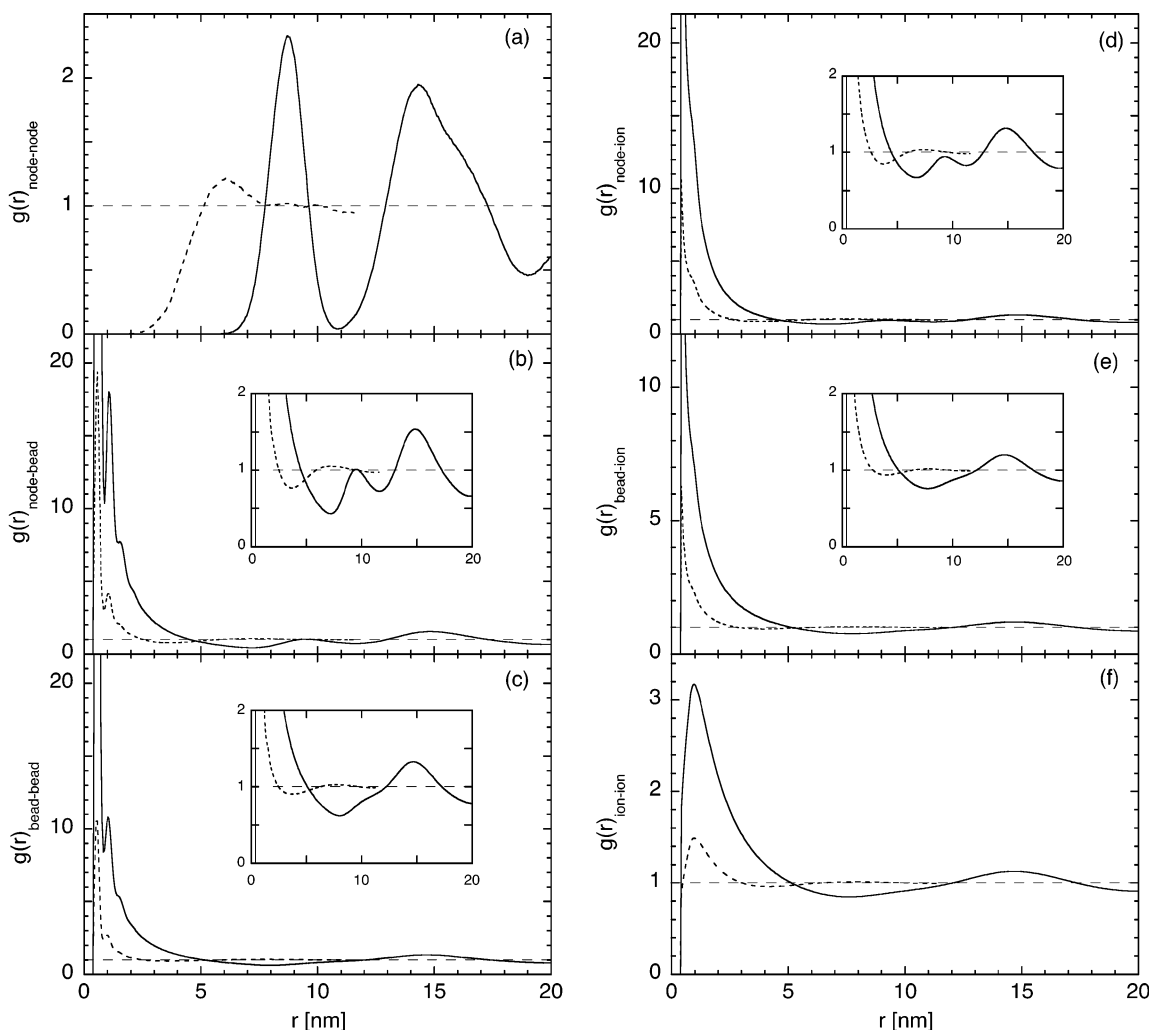


Figure 5. (a) Node–node, (b) node–bead, (c) bead–bead, (d) node–ion, (e) bead–ion, and (f) ion–ion radial distribution functions for the reference system at $\eta_{\text{network}} = 0.00137$ ($V \approx V_{\text{eq}}$) (solid curves) and 0.0072 ($V \approx V_{\text{eq}}/5$) (dashed curves) using the larger system size containing eight unit cells. At $\eta_{\text{network}} = 0.00137$, the maximum values of the radial distribution functions are (b) 91.9, (c) 49.9, (d) 51.0, and (e) 23.9.

the polyelectrolyte solution displays a minimum at approximately 0.30. Only at a very extreme dilution, $P/\rho k_B T$ will approach its ideal value 0.54 from below. This value is obtained by dividing the number of molecules (chains and counterions) by the total number particles.

To assess the system size dependence of the results, we performed simulations of systems containing eight unit cells instead of only one. The reduced pressures obtained from these simulations are shown in Figure 4a for the reference gel and in Figure 7a for system II. We found only very marginal differences (<0.03) in the reduced pressures for the two system sizes, indicating that the smaller system is sufficiently large for the determination of the thermodynamic properties.

In Figure 4b, the rms end-to-end distances, $\langle R_{\text{ee}}^2 \rangle^{1/2}$, of the chains in the polyelectrolyte gel and in a polyelectrolyte solution at the same densities are shown. At the largest packing fraction considered, the extensions of both the linear chain and the network chain are near that of a Gaussian chain [$\langle R_{\text{ee}}^2 \rangle^{1/2} = \langle R_{\text{bb}}^2 \rangle^{1/2} (N_{\text{bead}} - 1)^{1/2} \approx 2.5$ nm]. The network chains are slightly more contracted than the linear polyelectrolyte chains. Obviously, the topological constraint compresses the chains in the gel at high densities. The Gaussian chain approximation does not hold for the network chains in any wider range of packing fractions.

As the packing fraction is reduced, the end-to-end distance of the chains increases in both systems. In the gel, the chains

become strongly stretched due to the connectivity of the network, whereas in the polyelectrolyte solution $\langle R_{\text{ee}}^2 \rangle^{1/2}$ increases much slower and eventually levels off. In the infinite-dilution limit, $\langle R_{\text{ee}}^2 \rangle^{1/2} = 7.3$ nm was obtained from a separate simulation of a single polyion with $N_{\text{bead}} = 20$ and no counterions.

When the gel is in equilibrium with a reservoir of pure solvent (indicated by the arrow in Figure 4b), the rms end-to-end separation of the chains in the gel is 7.8 nm. This is larger than the extension of the single chain at infinite dilution, where the stretching is governed by the unscreened electrostatic repulsion among the charges. Hence, the observation $\langle R_{\text{ee}}^2 \rangle^{1/2}_{\text{polyelectrolyte gel}} > \langle R_{\text{ee}}^2 \rangle^{1/2}_{\text{single chain}}$ demonstrates that the direct electrostatic repulsion among the network charges alone is not sufficient to explain the swelling of the polyelectrolyte gel. Instead, the osmotic pressure from counterions, electrostatically confined in the gel, is the dominating contribution to the swelling. This issue was also discussed in our earlier work on the basis of properties of electrostatically coupled and uncoupled polyelectrolyte gels.¹²

Structural Properties of the Reference Gel. The structure of the reference gel at two different volumes has been characterized by means of radial distribution functions (rdf's). The rdf's, $g_{ij}(r)$, provide information on the relative density of particle j at distance r from particle i . At short separation where particles would overlap, $g_{ij}(r) = 0$, whereas in a fluid at large separations where a uniform distribution is achieved, $g_{ij}(r) = 1$ by definition.

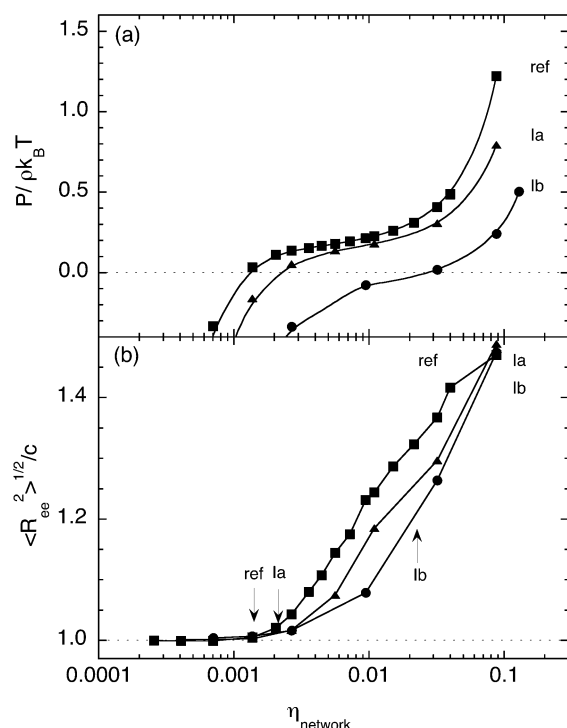


Figure 6. (a) Reduced pressure, $P/\rho k_B T$, and (b) normalized rms end-to-end chain distance, $\langle R_{ee}^2 \rangle^{1/2}/c$, as a function of the network packing fraction, η_{network} , for the reference system ($z_{\text{bead}} = 1$), system 1a ($z_{\text{bead}} = 0.5$), and system 1b ($z_{\text{bead}} = 0$). In part b, $\langle R_{ee}^2 \rangle^{1/2}$ is calculated for chains excluding the nodes but has been rescaled by the factor 21/19 and $c = \sqrt{3}(a/4)$ is the hypothetical node–node separation for nodes localized at the lattice sites of the diamond lattice with a denoting the length of the cubic unit cell. Packing fractions at which $P = 0$ are indicated by arrows.

Figure 5 displays the six different rdf's for the reference system utilizing the larger system size. The structure is given for two different packing fractions, viz. $\eta_{\text{network}} = 0.00137$ (solid curves) and 0.0072 (dashed curves). In the first case, $P/\rho k_B T = 0.032$ and hence the system is close to equilibrium with pure solvent ($V \approx V_{\text{eq}}$, see Figure 4a), whereas in the other case $V \approx V_{\text{eq}}/5$. The structure at V_{eq} will first be discussed, and thereafter the effect of the compression will be considered.

Figure 5a displays the node–node rdf. At $V \approx V_{\text{eq}}$, prominent peaks centered at $r \approx 8.7$ and 14 nm are observed. An integration of the rdf shows that the first peak involves 4 nodes, which are the 4 nearest neighbors linked to the central node by a single chain (see Figure 1). The second and broader peak involves 24 nodes, which are the 12 next nearest neighbors linked to the central node through two successive chains and the 12 following nodes linked to the central node by three successive chains and residing on the opposite side of the six-membered rings. For an ideal diamond lattice, the distances between the central node and these three different groups of nodes are $\sqrt{3}(a/4)$, $\sqrt{8}(a/4)$, and $\sqrt{11}(a/4)$, respectively, with a being the length of the unit cell (cf. Figure 1). With $a = L/2$ (eight unit cells in the box), distances of 8.66, 14.1, and 16.6 nm, respectively, are obtained for the ideal situation. The distance separation of the peaks from the two last groups of nodes is too small to give separated maxima in the node–node rdf, but a shoulder appears on the second peak at $r \approx 16.5$ nm. Thus, at equilibrium with pure solvent the defect-free network is sufficiently expanded to make the two first shells of nodes separated and the location of their maxima close to those of the ideal structure. The snapshot of the reference system given

in Table 2 also confirms the appearance of an expanded structure with extended six-rings.

The node–bead rdf is given in Figure 5b and displays the spatial correlation between a cross-linking node and the polyion beads. The four beads directly bonded to a node cause the first and very pronounced maximum, and the weaker second maximum arises from the following four beads. At increasing distance from the node along the chain, this spatial correlation becomes weaker and it is not possible to distinguish separate density maxima for the following beads in a chain. At intermediate distances ($r \approx 5\text{--}13$ nm), the rdf becomes smaller than one, which is related to the low bead densities inside a ring formed by six chains. However, a local maximum appears at $r \approx 9.5$ nm corresponding to the typical distance between two connected nodes and arises from the enhanced bead density around a neighboring node. A more prominent maximum appears at $r \approx 15$ nm, being related to the enhanced bead density near the three remaining nodes of a ring (cf. Figure 5a).

Figure 5c shows the bead–bead rdf. It possesses two clear maxima at short distances, arising from the bonded nearest and next nearest neighbors. Moreover, a long-range structure with an additional maximum at $r \approx 14.5$ nm is observed. The maximum at $r \approx 9.5$ nm appearing for the node–bead rdf is reduced to a shoulder, since in the bead–bead rdf the average is taken over the whole circumference of the ring and the locally enhanced density of beads near a node becomes less prominent.

The node–counterion and bead–counterion rdf's, shown in Figure 5d and e, respectively, display distinct maxima at contact separation $r = 0.4$ nm originating from a combination of the hard-sphere repulsion and the electrostatic attraction. Shoulders appear at $r \approx 0.8$ nm arising from counterions residing close to a neighboring bead or node. At longer separation, the ion distribution with respect to a node (Figure 5d) or a bead (Figure 5e) resembles those of the bead distribution with respect to a node (Figure 5b) or another bead (Figure 5c), respectively, but the correlations are weaker here.

Finally, Figure 5f provides the counterion–counterion rdf. Despite the mutual repulsion of the ions, the rdf possesses a considerable maximum at $r \approx 1.0$ nm. Moreover, a minimum appears at $r \approx 7$ nm and a subsequent maximum at $r \approx 15$ nm, consistent with a six-ring with a diameter of ≈ 15 nm dressed with counterions.

Thus, at equilibrium with pure solvent, the node–node rdf shows that the positions of the nodes are spatially strongly correlated. A high local density of beads near the nodes appears, and the counterions are preferentially located near the nodes and the beads. On a longer length scale, all the remaining distribution functions display a particle deficiency at $r \approx 5\text{--}13$ nm and a particle excess at $r \approx 13\text{--}17$ nm, supporting the existence of expanded six-rings formed by the chains as suggested from the node–node rdf and the snapshot in Table 2. Moreover, weaker local density maxima appear at $r \approx 9\text{--}10$ nm distance arising from six branches regularly placed on the circumference of the ring. These results clearly show that when the polyion network is in equilibrium with pure solvent, it is highly expanded and that a structure extending over several node separations (chain lengths) is present.

At the larger packing fraction (5-fold increase), the length of the box is reduced by a factor of 1.7. Generally, Figure 5 shows that the structure of the gel is strongly affected upon the compression. Figure 5a makes clear that there is only a spatial density correlation among nearest neighbor nodes, and parts b–e of Figure 5 show reduced amplitude of the initial peaks and fewer resolved peaks at longer separation. Since the reduction

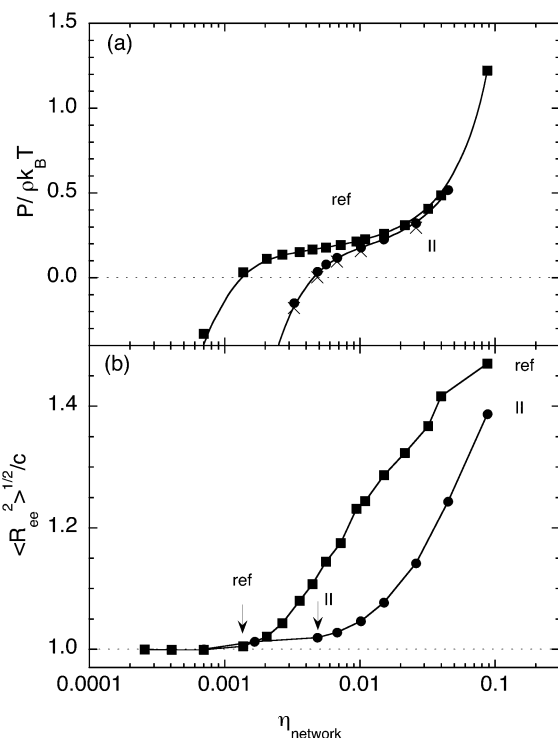


Figure 7. (a) Reduced pressure, $P/\rho k_B T$, and (b) normalized rms end-to-end chain distance, $\langle R_{\text{ee}}^2 \rangle^{1/2}/c$, as a function of the network packing fraction, η_{network} , for the reference system ($\chi_{\text{node}} = 0.050$) and system II ($\chi_{\text{node}} = 0.025$). In part a, pressures from an 8-fold larger gel system are also given (five crosses) but barely visible. For part b, see the legend of Figure 6 for further details.

of the amplitude of the rdf's at short separation is also about a factor of 5, the contact densities are unaffected by the compression. This is a typical feature for the accumulation of counterions at highly charged objects. All rdf's except the node-node rdf display a weak minimum at $r \approx 4$ nm. Considering that a ring has an expected diameter of $16.5/1.7$ nm ≈ 8 nm, a somewhat lower density at distances corresponding to the ring radius is still observed, although the density variation is strongly attenuated as compared to the more expanded gel. Finally, we notice that the density of the neutral gel in equilibrium with pure solvent is another factor 5 larger. Hence, for the neutral gel, structuring originating from the network topology is further reduced.

Thus, as the polyelectrolyte gel is compressed, the long-range inhomogeneous distributions of network particles and counterions are reduced and the relation to the gel topology is lost eventually. This is in contrast to the typical behavior for simple fluids where the structure continuously becomes more prominent as the density is increased.

Variation of the Chain Linear Charge Density. Figure 6a provides information on the influence of the linear charge density on the pressure, which displays the $P/\rho k_B T$ vs η_{network} relation for the reference system, the corresponding gel with a 2-fold reduced linear charge density (system Ia), and the corresponding uncharged gel (system Ib). It is seen that the same principal shape of the relation remains as the chain linear charge density is reduced. However, the pressure vs packing fraction curve is shifted to lower pressure/higher packing fraction as the network charges are reduced. Most noticeable is that the equilibrium network packing fractions, $\eta_{\text{network,eq}}$, differ 20-fold between the uncharged gel (system Ib) and the fully charged gel (reference system) (see also Table 3). Hence, the ability of a gel to swell in an excess of solvent is strongly affected by the

network charges and their counterions. Regarding the pressure, we recall that N_{ion} varies among the systems. Thus, N and hence also ρ are unequal at a given η_{network} , making the conversion factors between pressure and reduced pressure different among the systems.

Figure 6b shows the extension of the chains expressed by the normalized rms end-to-end distance, $\langle R_{\text{ee}}^2 \rangle^{1/2}/c$. In this type of representation, $c = \sqrt{3} (a/4)$ denotes the hypothetical node-node separation for nodes localized at the lattice sites of the diamond lattice, with a being the length of the cubic unit cell. Thus, $\langle R_{\text{ee}}^2 \rangle^{1/2}/c$ denotes the chain extension measured by the distance between nearest neighbor lattice points of the diamond lattice. The packing fractions, at which the systems are in equilibrium with pure solvent, are indicated by the arrows. At very low packing fractions, the chains are stretched and the rms end-to-end distance of the chains is equal to the distance between nearest neighbor lattice sites (cf. Figure 5a and the related discussion). At intermediate packing fractions, $\langle R_{\text{ee}}^2 \rangle^{1/2}/c$ increases for all the gels. The onset of the increase of $\langle R_{\text{ee}}^2 \rangle^{1/2}/c$ appears at lower packing fraction for chains with a higher charge density. The magnitude of this increase is dependent on the chosen topology. We expect it to be large for the diamond lattice selected, since there are large empty spaces in the swollen gel (see Figure 1) that can be filled when the chains become less stretched. At very high packing fractions, $\langle R_{\text{ee}}^2 \rangle^{1/2}/c$ becomes less dependent on the linear charge density. This is most likely an effect of the electrostatic interactions becoming more screened and the excluded volume effects becoming more important.

The affine assumption implies that $\langle R_{\text{ee}}^2 \rangle^{1/2}/c$ should be independent of η_{network} . In equilibrium with pure solvent, this condition is fulfilled for the reference gel and gel Ia (see arrows in Figure 6b) but becomes questionable as soon as the osmotic pressure is increased. For the uncharged gel, however, the affine approximation does not hold for any nonnegative pressure.

Variation of the Cross-Linking Density. Figure 7a shows the reduced pressure vs packing fraction relations for a gel with a 2-fold higher cross-linking density (system II) and that of the reference system. The shorter chain length obtained at the higher cross-linking density leads to a more negative pressure at low packing fractions and to a less developed intermediate regime. The equilibrium network packing fraction, $\eta_{\text{network,eq}}$, is increased by a factor 3.4 (Table 3). Thus, the cross-linking density of the polymer network influences the equilibrium volume, and as expected, the swelling ability of a more cross-linked gel is smaller. At high packing fractions, the pressures of the two gels are virtually identical.

The chain extensions of the two systems are given in Figure 7b. Similarly to the reference system, in system II, which has a higher cross-linking density, $\langle R_{\text{ee}}^2 \rangle^{1/2}/c$ starts to deviate from unity at $\sim V_{\text{eq}}$. The affine approximation should also be valid here for the network being in equilibrium with a reservoir of pure solvent. At high packing fractions, $\langle R_{\text{ee}}^2 \rangle^{1/2}/c$ for the reference system and system II approach each other.

Moreover, for the two investigated systems at $P/\rho k_B T \approx 0$, the scaling of $\langle R_{\text{ee}}^2 \rangle^{1/2}$ follows the relation $\langle R_{\text{ee}}^2 \rangle^{1/2} \sim n_{\text{bead}}^\alpha$ with $\alpha = 1$. This demonstrates that the chains are stretched at $P/\rho k_B T \approx 0$.

Variation of the Chain Flexibility. The influence of the chain stiffness on the pressure in the gel has also been examined. Figure 8a displays the pressure vs packing fraction data for gels formed by chains with two different flexibilities (systems IIIa and b) as well as for the reference system. The persistence lengths of the corresponding uncharged chains are 4.0 and 37

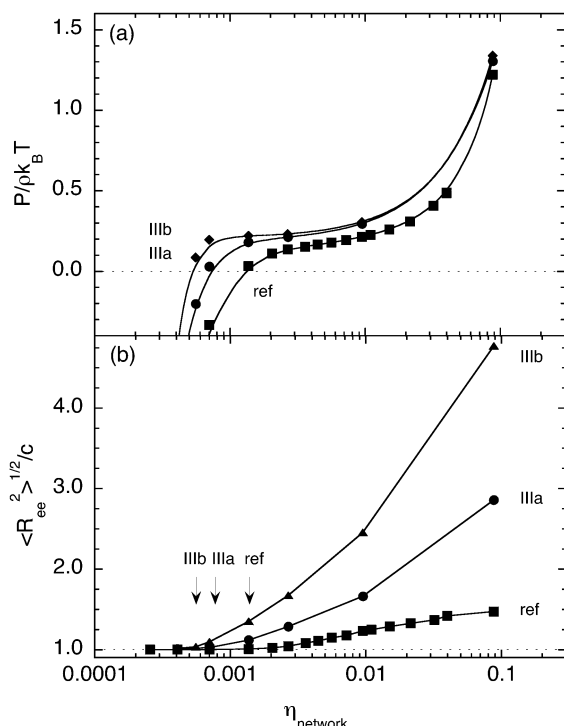


Figure 8. (a) Reduced pressure, $P/(\rho k_B T)$, and (b) normalized rms end-to-end chain distance, $\langle R_{ee}^2 \rangle^{1/2}/c$, as a function of the network packing fraction, η_{network} , for the reference system ($l_p = 0.7$ nm), system IIIa ($l_p = 4.0$ nm), and system IIIb ($l_p = 37$ nm). For part b, see the legend of Figure 6 for further details.

nm, respectively, as compared to 0.70 nm for the reference system. Generally, for a given packing fraction the reduced pressure becomes larger as the chain stiffness is increased and the equilibrium network packing fraction, $\eta_{\text{network,eq}}$, is decreased approximately 2 or 3 times relative to that of the reference system, the largest increase appearing at the initial stiffening of a flexible chain (Table 3). The intermediate pressure range, in which the reduced pressure only increases weakly, becomes more extended. The enhanced swelling ability displayed by the gel with stiffer chains is attributed to the smaller loss of configurational entropy upon the imposed stretching.

In Figure 8b, the normalized rms end-to-end distances of the stiff polymer chains, IIIa and b, and that of the flexible chains in the reference system are given as a function of the packing fraction. At small packing fractions, the chains are equally stretched in all three systems. As the packing fraction is increased, $\langle R_{ee}^2 \rangle^{1/2}/c$ increases more rapidly for the stiffer chains. This shows that the reduction of the chain extension is smaller for the stiffer chains when the system is compressed. The extended chains can obviously also be accommodated in a very compressed gel, when the node–node separation of an ideal diamond-like lattice is much smaller than $\langle R_{ee}^2 \rangle^{1/2}$.

As for the reference system, $\langle R_{ee}^2 \rangle^{1/2}/c$ is essentially independent of η_{network} at $P = 0$, showing that the affine assumption holds when gels composed of the stiffer chains are in equilibrium with pure solvent. However, the affine approximation becomes questionable at smaller compressions for these gels, compared to gels made from more flexible chains (see arrows in Figure 8b).

We will now consider the distribution of the end-to-end distances, $P_{\text{chain}}(R_{ee})$, averaged over all chains for systems IIIa and b at the same volume fraction near $P/(\rho k_B T) = 0$ ($\eta_{\text{network}} = 5.6 \times 10^{-4}$) and at a compressed state ($\eta_{\text{network}} = 9.4 \times 10^{-3}$), which is shown in Figure 9. Starting with the volume near the

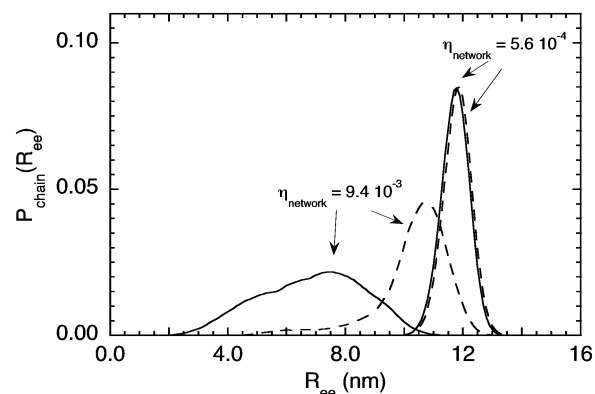


Figure 9. Average end-to-end distribution functions, $P_{\text{chain}}(R_{ee})$, for system IIIa (solid curves) and IIIb (dashed curve) at the indicated η_{network} .

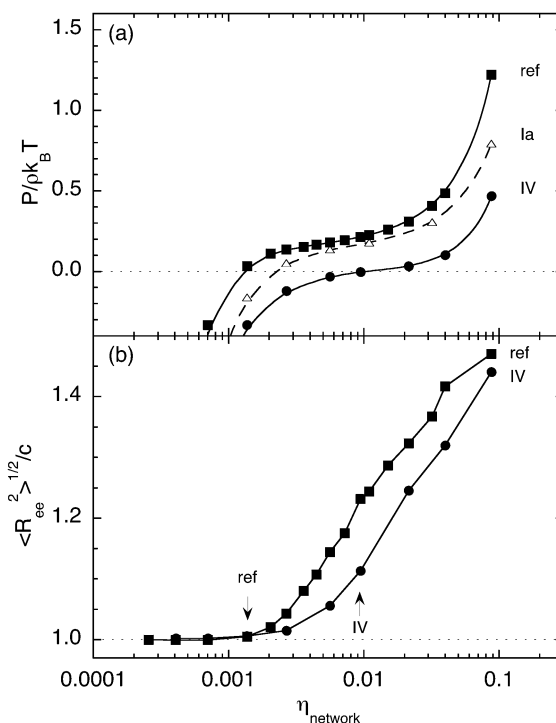


Figure 10. (a) Reduced pressure, $P/(\rho k_B T)$, and (b) normalized rms end-to-end chain distance, $\langle R_{ee}^2 \rangle^{1/2}/c$, as a function of the network packing fraction, η_{network} , for the reference system ($z_{\text{ion}} = -1$) and system IV ($z_{\text{ion}} = -2$). For part b, see the legend of Figure 6 for further details.

equilibrium with pure solvent, we see that the chain end-to-end distance distributions are essentially identical despite their very different bare persistence lengths, 4.0 and 37.0 nm, respectively. In the highly compressed state, however, the stiffer chains are only somewhat less expanded, whereas the extension of the more flexible ones is considerably reduced. The very similar distributions in the swollen state indicate that the structures of the networks are similar at the same given volume. A comparison between any gel (except for gel II) and the reference system at the equilibrium volume of the reference system displays again nearly identical chain end-to-end distribution functions. Hence, factors as charge and chain stiffness strongly affect the equilibrium volume, but for a swollen gel at a given volume the network structures are very similar.

Variation of Counterion Valence. In Figure 10a, the pressure–packing fraction relation for system IV containing divalent counterions and that of the reference system is shown. The increase of the counterion valence leads to a shift to lower

reduced pressure/higher packing fraction, similar to that obtained with decreasing linear charge density of the chains. The intermediate regime of a highly compressible gel is, however, still extended and appears at $P/\rho k_B T \approx 0$. The equilibrium network packing fraction, $\eta_{\text{network,eq}}$, is increased nearly 1 order of magnitude and differs only with a factor of 3 as compared to the uncharged gel (Table 3). As in Figure 6, the ρ - η_{network} relations differ among the systems.

Figure 10a also shows the pressure vs packing fraction relation of system Ia (open symbols). The comparison of the data of systems Ia and IV, which are related to each other by the charge rescaling $z_i \rightarrow 2z_i$, shows that an increased electrostatic interaction leads to a lower pressure. In the more highly charged system, the counterions are more strongly bound to the network chains causing the decrease in pressure.

In Figure 10b, $\langle R_{\text{ee}}^2 \rangle^{1/2}/c$ of system IV and of the reference system is given as a function of η_{network} . At equal η_{network} , the extension of the chains is smaller for the system containing divalent counterions, which can be explained by a smaller osmotic contribution from the counterions owing to a fewer number of them and a stronger electrostatic attraction to the network, as compared to monovalent counterions. At equilibrium with pure solvent (see arrow for system IV in Figure 10b), $\langle R_{\text{ee}}^2 \rangle^{1/2}$ does not scale linearly with the length of the simulation box, and thus, the affine assumption is not valid under these conditions.

Comparison with Experiments. Experimentally, the swelling of a gel is often expressed in terms of equilibrium expansion, Q_{eq} , denoting the ratio of the volume of the swollen gel and the volume of the corresponding dry gel. For polyelectrolyte gels, Q_{eq} is typically 10^2 – 10^3 , whereas for uncharged gels it is approximately 10^1 .^{48,49} In this respect, the present model is able to predict the large difference of the swelling ratios between uncharged charged gels as well as realistic magnitudes of the swelling ratios (see Table 3).

The predicted trends in gel swelling are also consistent with experimental results. Experiments in salt-free solutions are scarce, but it is possible to compare the simulation results with experiments at low and constant ionic strength. The effect of an increased osmotic pressure at constant ionic strength was investigated by Fernández-Nieves et al.¹⁰ Here, the deswelling of polyelectrolyte microgel particles was induced by the addition of dextran to the reservoir. For example, in a 20% solution of dextran (500 kDa), a pressure of about 150 kPa can be achieved.⁵⁰

(i) The effect of the linear charge density was examined by Okay et al., who copolymerized sodium acrylate (NaAc) and N,N'-methylenebis(acrylamide). They found a substantially increased gel swelling when the amount of NaAc was increased.¹³ Their experiments were carried out in pure water and at low salt concentrations. It is not obvious, though, how the pH and thus the charge density were controlled in this study. (ii) The influence of the cross-linking density on the swelling of the gel was investigated by Loxley et al.⁵¹ They demonstrated that additional cross-linking reduces the gel volume in the swollen state but does not have any influence on the volume in the collapsed state. The swelling was induced by changing the pH and thereby the charge density of the titrating polymer. (iii) The influence of the chain stiffness on the swelling behavior has not yet been investigated experimentally. (iv) A decrease in gel volume for divalent counterions was observed by Liu et al.⁵²

Thus, there is a good qualitative agreement between our model predictions and experimental results, suggesting that the

model that we used contains the essential features for describing characteristic properties of polyelectrolyte gels.

Conclusions

Properties of model systems representing cross-linked polyelectrolyte gels have been determined by canonical Monte Carlo simulations. The gel was represented by a defect-free three-dimensional network having a diamond-like topology composed of charged beads and charged tetrafunctional nodes plus counterions. Electrostatic interactions and the connectivity of the network, which are two key issues determining the swelling of gels in a good solvent, are directly considered in the model.

On the basis of the analysis of thermodynamical and structural data, the main findings and conclusions to be drawn are as follows.

(A) The reduced pressure vs packing fraction relation for a charged gel displays three characteristic regions. At high packing fractions, the reduced pressure decreases rapidly as η_{network} is decreased due to a reduction of the hard-core pressure contribution. The reduced pressure also decreases at low packing fractions due to chain stretching, framing an intermediate region where the reduced pressure is slowly varying.

(B) In a swollen polyelectrolyte gel, charged network particles and counterions are inhomogeneously distributed in space with the counterions strongly accumulated near the network particles. For the defect-free network, the particle distribution reflects the underlying network topology. In the compressed state, the spatial correlations become strongly attenuated.

(C) The osmotic pressure arising from the entropy of the counterions is more important than the screened Coulomb repulsion among the network charges for the swelling behavior of the polyelectrolyte gel. In fact, the electrostatic correlations inside the gel give rise to a contractive contribution.¹²

(D) The polyelectrolyte gel becomes more swollen at (i) increasing chain linear charge density, (ii) decreasing cross-linking density, (iii) increasing chain stiffness, and (iv) decreasing counterion valence.

(E) The assumption of Gaussian statistics often employed in gel theories is not applicable for polyelectrolyte gels. The affine assumption, nevertheless, appears to be reasonable in most cases when the osmotic pressure of the polyelectrolyte gel is close to zero, but it becomes questionable at higher osmotic pressures.

(F) The simple coarse-grain model displays properties in good agreement with experimental trends, verifying that the model includes the most important elements for describing a polyelectrolyte gel. This gives us confidence that it will be possible to investigate the influence of many other factors, e.g., network imperfection (unequal chain lengths, dangling tails, loops, and entanglements), salt, and solvent quality on the equilibrium volume and the structure of the gel relevant for experimental gel systems. Finally, the study of the interaction between the gel and host molecules would bring the model system even closer to gel systems of technical relevance.

Acknowledgment. We are grateful for valuable discussions with Luca Bemporad, Lennart Lindfors, and Lennart Piculell. This work was financially supported by the Centre for Amphiphilic Polymers from Renewable Resources (CAP).

References and Notes

- (1) *Advances in Polymer Science*; Dušek, K., Ed.; Springer-Verlag: New York, 1993; Vols. 109 and 110.
- (2) Michaeli, I.; Katchalsky, A. *J. Polym. Sci.* **1957**, *23*, 683.
- (3) Katchalsky, A.; Michaeli, I. *J. Polym. Sci.* **1955**, *15*, 69.
- (4) Hansson, P. *Langmuir* **1998**, *14*, 2269.

- (5) Ashbaugh, H. S.; Piculell, L.; Lindman, B. *Langmuir* **2000**, *16*, 2529.
- (6) Sjöström, J.; Piculell, L. *Colloids Surf. A* **2001**, *183*–185, 429.
- (7) Hansson, P.; Schneider, S.; Lindman, B. *Prog. Colloid Polym. Sci.* **2000**, *115*, 342.
- (8) Hansson, P.; Schneider, S.; Lindman, B. *J. Phys. Chem. B* **2002**, *106*, 9777.
- (9) Fernández-Nieves, A.; Fernández-Barbero, A.; Vincent, B.; de las Nieves, F. J. *Macromolecules* **2000**, *33*, 2114.
- (10) Fernández-Nieves, A.; Fernández-Barbero, A.; Vincent, B.; de las Nieves, F. J. *Prog. Colloid Polym. Sci.* **2000**, *115*, 134.
- (11) Flory, P. J. *Principles of polymer chemistry*; Cornell University Press: Ithaca, NY, 1953.
- (12) Schneider, S.; Linse, P. *Eur. Phys. J. E* **2002**, *8*, 457.
- (13) Okay, O.; Sariisik, S. B. *Eur. Polym. J.* **2000**, *36*, 393.
- (14) Hansson, P. *Langmuir* **1998**, *14*, 4059.
- (15) Khokhlov, A. R.; Kramarenko, E. Y.; Makhaeva, E. E.; Starodubtzev, S. G. *Macromolecules* **1992**, *25*, 4779.
- (16) Flory, P. J.; Rehner, J. J. *J. Chem. Phys.* **1943**, *11*, 512.
- (17) Flory, P. J.; Rehner, J. J. *J. Chem. Phys.* **1943**, *11*, 521.
- (18) Wall, F. T. *J. Chem. Phys.* **1943**, *11*, 527.
- (19) James, H. M.; Guth, E. *J. Chem. Phys.* **1943**, *11*, 455.
- (20) James, H. M.; Guth, E. *J. Chem. Phys.* **1947**, *15*, 669.
- (21) Edwards, S. F.; Vilgis, T. A. *Rep. Prog. Phys.* **1988**, *51*, 243.
- (22) Everaers, R. *Eur. Phys. J. B* **1998**, *4*, 341.
- (23) Flory, P. J.; Erman, B. *Macromolecules* **1982**, *15*, 800.
- (24) Erman, B.; Flory, P. J. *Macromolecules* **1982**, *15*, 806.
- (25) Kenkare, N. R.; Hall, C. R.; Khan, S. A. *J. Chem. Phys.* **1999**, *110*, 7556.
- (26) Rubinstein, M.; Panyukov, S. *Macromolecules* **1997**, *30*, 8036.
- (27) Khokhlov, A. R.; Starodubtzev, S. G.; Vasilevskaya, V. V. Conformational transitions in polymer gels: theory and experiment. In *Advances in Polymer Science*; Dusek, K., Ed.; Springer-Verlag: New York, 1993; Vol. 109; p 123.
- (28) Escobedo, F. A.; de Pablo, J. J. *Phys. Rep.* **1999**, *318*, 85.
- (29) Escobedo, F. A.; de Pablo, J. J. *J. Chem. Phys.* **1999**, *110*, 1290.
- (30) Aydt, E. M.; Hentschke, R. *J. Chem. Phys.* **2000**, *112*, 5480.
- (31) Gilra, N.; Cohen, C.; Panagiotopoulos, A. Z. *J. Chem. Phys.* **2000**, *112*, 6910.
- (32) Aalberts, D. P. *J. Chem. Phys.* **1996**, *104*, 4309.
- (33) Barenbrug, T. M. A. O. M.; Smit, J. A. M.; Bedeaux, D. *Macromolecules* **1997**, *30*, 605.
- (34) Barenbrug, T. M. A. O. M.; Bedeaux, D.; Smit, J. A. M. *Macromolecules* **1999**, *32*, 199.
- (35) Escobedo, F. A.; de Pablo, J. J. *J. Chem. Phys.* **1997**, *106*, 793.
- (36) Ewald, P. P. *Ann. Phys.* **1921**, *64*, 253.
- (37) Allen, M. P.; Tildesley, D. J. *Computer Simulations of Liquids*; Oxford University Press: Oxford, 1989.
- (38) Limbach, H. J.; Holm, C. *J. Chem. Phys.* **2001**, *114*, 9674.
- (39) Lobaskin, V.; Linse, P. *J. Chem. Phys.* **1999**, *111*, 4300.
- (40) Frusawa, H.; Hayakawa, R. *Phys. Rev. E* **1998**, *58*, 6145.
- (41) Akinchina, A.; Linse, P. *Macromolecules* **2002**, *35*, 5183.
- (42) Ullner, M. *Macromolecules* **2002**, *35*, 1437.
- (43) Metropolis, N. A.; Rosenbluth, A. W.; Rosenbluth, M. N.; Teller, A.; Teller, E. *J. Chem. Phys.* **1953**, *21*, 1087.
- (44) Lobaskin, V.; Linse, P. *J. Chem. Phys.* **1998**, *109*, 3530.
- (45) Kolafa, J.; Perram, J. W. *Mol. Sim.* **1992**, *9*, 351.
- (46) Escobedo, F. A.; de Pablo, J. J. *J. Chem. Phys.* **1995**, *102*, 2636.
- (47) Linse, P. *MOLSIM*, 3.1.8 ed.; Lund University: Lund, 2001.
- (48) Philippova, O. E.; Hourdet, D.; Audebert, R.; Khokhlov, A. R. *Macromolecules* **1997**, *30*, 8278.
- (49) Tanaka, T.; Fillmore, D.; Sun, S.-T.; Nishio, I.; Swislow, G.; Shah, A. *Phys. Rev. Lett.* **1980**, *45*, 1636.
- (50) Livney, Y. D.; Ramon, O.; Kesselman, E.; Cogan, U.; Mizrahi, S.; Cohen, Y. *J. Polym. Sci. Part B: Polym. Phys.* **2001**, *39*, 2740.
- (51) Loxley, A.; Vincent, B. *Colloid Polym. Sci.* **1997**, *275*, 1108.
- (52) Liu, X.; Tong, Z.; Hu, O. *Macromolecules* **1995**, *28*, 3813.